

RESEARCH ARTICLE

Absence of UCHL1 function leads to selective motor neuropathy

Barış Genç^{1,a}, Javier H. Jara^{1,a}, Megan C. Schultz¹, Marin Manuel^{2,3}, Macdonell J. Stanford¹, Mukesh Gautam¹, Jodi L. Klessner¹, Gabriella Sekerkova², Daniel B. Heller¹, Gregory A. Cox⁴, Charles J. Heckman^{5,6}, Christine J. DiDonato^{7,8} & P. Hande Özdinler^{1,9,10}

¹Department of Neurology and Clinical Neurological Sciences, Northwestern University, Feinberg School of Medicine, Chicago, Illinois, USA

²Department of Physiology, Northwestern University, Feinberg School of Medicine, Chicago, Illinois, USA

³UMR 8119 CNRS/Paris, Descartes University, Paris, France

⁴The Jackson Laboratory, Bar Harbor, Maine, USA

⁵Department of Medicine and Rehabilitation, Northwestern University, Feinberg School of Medicine, Chicago, Illinois, USA

⁶Department of Physical Therapy and Movement Sciences at Northwestern University, Feinberg School of Medicine, Chicago, Illinois, USA

⁷Department of Pediatrics, Feinberg School of Medicine, Northwestern University, Chicago, Illinois, USA

⁸Human Molecular Genetics Program, Ann & Robert H. Lurie Children's Hospital of Chicago Research Center, Chicago, Illinois, USA

⁹Robert H. Lurie Cancer Center, Northwestern University, Chicago, Illinois, USA

¹⁰Cognitive Neurology and Alzheimer's Disease Center, Northwestern University, Chicago, Illinois, USA

Correspondence

P. Hande Özdinler, Department of Neurology and Clinical Neurological Sciences, Northwestern University, Feinberg School of Medicine, Chicago 60611, IL.
Tel: +1-312-5032774; Fax: +1-312-5030872;
E-mail: ozdinler@northwestern.edu

Funding Information

This work was supported by grants from National Institutes of Health-R01NS085161-01 (P.H.O.), Les Turner ALS Foundation, Wenske Foundation (P.H.O.), P30 NS054850-01A1 (C.J.H.); R01NS060926 and MDA 255785 (C.J.D.) National Institutes of Health (5T32AG020506-09 M.A.D. Postdoctoral Training; B.G.), and ALSA Safenowitz fellowship (J.H.J. and M.M.), by the Northwestern University Mouse Histology and Phenotyping Laboratory and a Cancer Center Support Grant (NCI CA060553) and Northwestern University's Center for Advanced Microscopy and a Cancer Center Support Grant (NCI CA060553).

Received: 4 December 2015; Revised: 29 January 2016; Accepted: 8 February 2016

Annals of Clinical and Translational Neurology 2016; 3(5): 331–345

doi: 10.1002/acn3.298

^aThese authors contributed equally.

Abstract

Objective: The aim of this study was to investigate the role of ubiquitin C-terminal hydrolase-L1 (UCHL1) for motor neuron circuitry and especially in spinal motor neuron (SMN) health, function, and connectivity. **Methods:** Since mutations in *UCHL1* gene leads to motor dysfunction in patients, we investigated the role of UCHL1 on SMN survival, axon health, and connectivity with the muscle, by employing molecular and cellular marker expression analysis and electrophysiological recordings, in healthy wild-type and *Uchl1^{nm3419}* (*UCHL1*−/−) mice, which lack all UCHL1 function. **Results:** There is pure motor neuropathy with selective degeneration of the motor, but not sensory axons in the absence of UCHL1 function. Neuromuscular junctions (NMJ) are impaired in muscle groups that are innervated by slow-twitch or fast-twitch SMN. However, unlike corticospinal motor neurons, SMN cell bodies remain intact with no signs of elevated endoplasmic reticulum (ER) stress. **Interpretation:** Presence of NMJ defects and progressive retrograde axonal degeneration in the absence of major SMN soma loss suggest that defining pathology as a function of neuron number is misleading and that upper and lower motor neurons utilize UCHL1 function in different cellular events. In line with findings in patients with mutations in *UCHL1* gene, our results suggest a unique role of UCHL1, especially for motor neuron circuitry. SMN require UCHL1 to maintain NMJ and motor axon health, and that observed motor dysfunction in the absence of UCHL1 is not due to SMN loss, but mostly due to disintegrated circuitry.

Introduction

To date five different patients are identified with mutations in their ubiquitin C-terminal hydrolase-L1 (UCHL1) gene. The first two patients displayed Parkinson-like symptoms, with defects in their motor function and spasticity in the legs.¹ Recently, three siblings with very early neurodegeneration associated with upper motor neuron dysfunction were identified to have Glu7Ala mutation in their *UCHL1* gene.² These clinical reports sparked interest in exploring the role of UCHL1 function for motor neuron circuitry and motor neuron diseases, especially the ones in which voluntary movement is impaired.

UCHL1 is critically important for protein homeostasis due to its dual hydrolase and ligase functions, by adding or removing ubiquitin to poly-ubiquitin chains.^{1,3–5} This is a unique ability of UCHL1 in maintaining free ubiquitin levels and a central role within the ubiquitin proteasome system (UPS) in neurons.⁶ Defects in protein turnover and UPS has been closely associated with motor neuron diseases, and it is suggested that motor neurons heavily depend on the proper function of the UPS.^{7–11} Therefore, investigating the role of UCHL1, especially for motor neurons, and within the context of motor neuron diseases is important.

To date numerous mouse models are developed and they revealed important information about the involvement of UCHL1 in both neurodegeneration and cellular proliferation.^{12–15} For example, the UCHL1 knockout mouse with a targeted deletion of the exons 6 through 8 of the UCHL1 gene showed its requirement for the normal structure and function of the neuromuscular junctions (NMJ).¹² In line with reports that demonstrate motor dysfunction in *Uchl1^{nm3419}* (UCHL1^{–/–}) mice, which lack all UCHL1 function,¹⁵ we recently defined a unique importance of UCHL1 for motor neuron circuitry.¹⁶ Mice that lacked UCHL1 developed motor dysfunction as early as postnatal day (P) 40, and corticospinal motor neurons (CSMN) displayed an early and profound degeneration with spine loss and disintegration of apical dendrites. However, the role of UCHL1 on the spinal component of motor neuron circuitry remained elusive.

To reveal the potential link between UCHL1 function and motor circuitry, we investigated spinal motor neuron

(SMN) health and connectivity using electrophysiology, histology and molecular marker expression analysis in healthy as well as diseased mice that lacked all UCHL1 function. Our findings revealed defects in the motor, but not the sensory branch of the femoral nerve and disintegration of NMJ. Interestingly, despite early and profound CSMN degeneration, SMN soma remained intact in the spinal cord. NMJ in soleus, and extensor digitorum longus (EDL) muscles, which are mainly innervated by slow-twitch and fast-twitch SMN, respectively, display profound disintegration in the absence of UCHL1 function. *In vivo* recordings further delineate the early functional defects even when neurons are intact and display no signs of increased endoplasmic reticulum (ER) stress or neuron loss. Altogether, our studies suggest that UCHL1 plays different roles in CSMN and SMN and that circuitry defects are more relevant to developing disease pathologies in the absence of UCHL1.

Materials and Methods

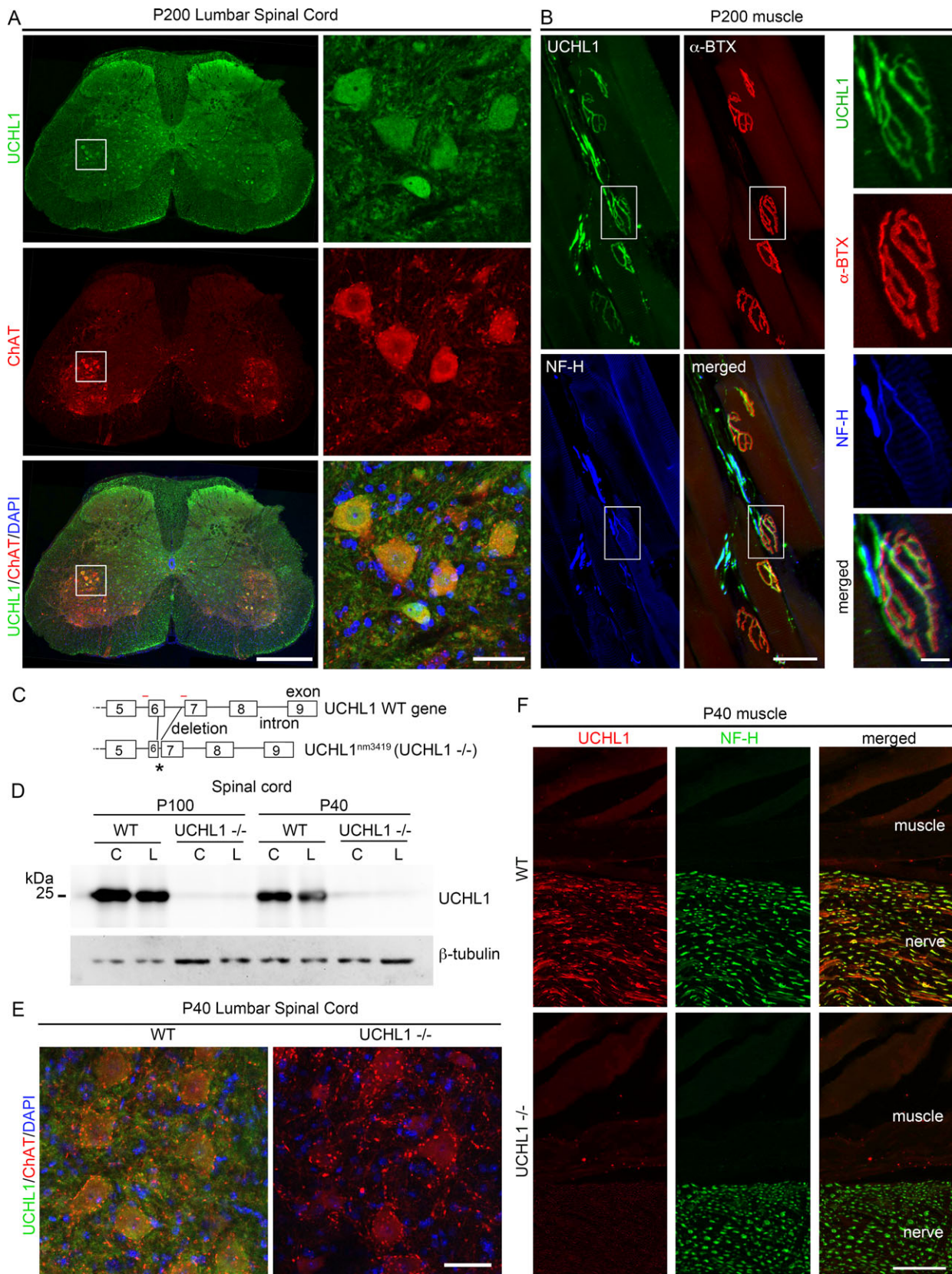
Mice

All animal procedures were approved by Northwestern University Animal Care and Use Committee, and conformed to the standards of the National Institutes of Health. *Uchl1^{nm3419}* (UCHL1^{–/–}) mice identified by G. Cox at The Jackson Laboratory carry a spontaneous 795 base-pair intragenic deletion that results in the removal of the final 24 base-pair of exon 6 and the first 771 base-pairs of intron 6¹⁵ (Fig. 1C). Heterozygous mice (UCHL1^{+/-}) were viable, fertile, and were bred together to generate UCHL1 deficient (UCHL1^{–/–}) mice. All mice were on the C57BL/6J background. Survival times and motor function defects were comparable between males and females with 100% penetrance. Primers used to determine genotype are UCHL1 forward: tggacggctgtgtgctaatg, WT reverse: ctaagggaagggctctgctcatc, mutant (Mt) reverse: gtcatctacctaagagagccaag, yielding 668 bp WT and 334 bp Mt PCR products.

Tissue collection and histology

Mice were deeply anesthetized with ketamine (90 mg/kg) and xylazine (10 mg/kg) and perfused with 4% PFA in

Figure 1. UCHL1 is expressed in wild-type SMN and is absent in UCHL1^{–/–} mice. (A) UCHL1 protein is expressed in SMN (ChAT+ neurons) in the spinal cord. (B) Parallel sections of gastrocnemius muscle from WT mice at P40. UCHL1 (green) colocalizes with SMN axons (NF-H, blue) and α -BTX (red). Boxed areas are enlarged to the side. (C) Drawing of *Uchl1* gene in WT and UCHL1 deficient (*Uchl1^{nm3419}*; UCHL1^{–/–}) mice. Partial deletions of exon 6 and intron 6 sequences cause a frameshift and create a *de novo* stop codon (*). Red lines = location of PCR primers. (D) There is no UCHL1 protein in the spinal cord of UCHL1^{–/–} mice by western blot analysis. β -tubulin is used as loading control. (E) UCHL1 expression cannot be detected in the UCHL1^{–/–} spinal cord by immunocytochemistry. (F) UCHL1 is not expressed in the muscle of WT or UCHL1^{–/–} mice. UCHL1 expression colocalizes with the axons. C: cervical; L: lumbar; Scale bars: A = 50 μ m, B = 50 μ m, B enlarged = 10 μ m, E = 200 μ m, E enlarged = 50 μ m, F = 50 μ m. BTX, bungarotoxin.



PBS. Spinal cords were removed intact, and gastrocnemius, soleus and EDL muscles were isolated. All tissue were postfixed by 4% PFA overnight, and kept in PBS-sodium azide (0.01%) at 4°C. Spinal cords were sectioned 50- μ m thick using a vibrating microtome (VT1000S, Leica Instruments, Nussloch, Germany). Soleus, EDL and gastrocnemius muscles were cryoprotected, and 30- μ m-thick serial sections were collected in a cryostat parallel to the muscle fiber. Gastrocnemius muscle was dehydrated in alcohol series, embedded in paraffin, and 4- μ m-thick cross sections were collected at the Northwestern University Mouse Histology and Phenotyping Laboratory ($n = 3$ for P40, P65, P80, and P100). Nissl, hematoxylin–eosin (H&E), and nonspecific esterase staining (NSE) staining were performed as previously described.¹⁷ Motor and sensory branches of the femoral nerve and the ventral roots were isolated at P200 ($n = 3$), postfixed in 4% PFA in sodium cacodylate buffer, and 1- μ m-thick sections were collected and stained with toluidine blue at the Northwestern University Center for Advanced Microscopy and analyzed as previously described.¹⁸

Western blot

Spinal cords were isolated from WT and UCHL1 $^{-/-}$ mice deeply anesthetized with ketamine (90 mg/kg) and xylazine (10 mg/kg) at P40 and P100. Cervical and lumbar spinal cords were quickly dissected in cold PBS. Tissue was homogenized in 1 mL of T-PER (Tissue Protein Extraction Reagent, Pierce, Rockford, IL) supplemented with protease inhibitor cocktail (Calbiochem, Billerica, MA). The supernatants were collected after centrifugation (17,000 g, 10 min., 4°C). Total protein lysate (10 μ g; determined by BCA Kit; Pierce, Rockford, IL) were resolved by 10% SDS-PAGE, transferred onto a PVDF membrane (Bio-Rad, Hercules, CA), and immunoblotted with primary antibodies overnight at 4°C. The following primary antibodies were used: anti-UCHL1 (1:2000; ProteinTech, Rosemont, IL, cat # 14730-1-AP, lot # 00024921) and anti- β tubulin (1:5000; Abcam, cat # AB21057, lot # 959864). The membranes were stripped with 0.2N NaOH for 10 min and washed with PBS-T. Blots were developed by enhanced chemiluminescence (Millipore, Temecula, CA) using HRP conjugated secondary antibodies. For pJNK, and JNK western blots, spinal cords were isolated from WT and UCHL1 $^{-/-}$ mice at P100. Lumbar spinal cords were quickly dissected in dissociation solution. Tissue was homogenized in 600 μ l lysis buffer (10 mmol/L Tris-HCL, pH 7.5, 1.0% Triton X-100, 145 mmol/L NaCl, and 5 mmol/L EDTA) supplemented with HALT Protease Inhibitor Cocktail (Thermo Scientific, Grand Island, NY). The supernatants were collected after centrifugation (14,000 rpm, 30 min.,

4°C). Total protein lysates (10 μ g; determined by BCA Kit; Pierce, Rockford, IL) were resolved by 7.5% SDS-PAGE, transferred onto a nitrocellulose membrane (GE Healthcare Life Sciences, Marlborough, MA), and immunoblotted with primary antibodies overnight at 4°C. The following primary antibodies were used: anti-UCHL1 (1:1000; ProteinTech, Rosemont, IL, cat # 14730-1-AP, lot # 00024921), anti-JNK (1:250; Cell-Signaling, Danvers, MA, cat # 9252S, lot # 15), anti-pJNK (1:1,000, Cell Signaling, Danvers, MA, cat # 4668S, lot # 11), and anti-actin (1:1,000; Millipore, Temecula, CA, cat # MAB1501R, lot # 2521458). The membranes were stripped with Restore PLUS Western Blot Stripping Buffer (Thermo Scientific, Grand Island, NY) for 30 min at 37°C and washed with PBS-T. Blots were developed by enhanced chemiluminescence (Thermo Scientific, Grand Island, NY) using HRP-conjugated secondary antibodies.

Immunocytochemistry

Immunocytochemistry was performed on every 6th section of mouse spinal cords, and on continuous serial sections for soleus, and EDL muscle. Primary antibodies were purchased from Millipore unless otherwise stated. Antibodies: anti-ChAT (choline acetyltransferase) (1:500, cat # AB144, lot # 2234133); anti-UCHL1 (1:1000; ProteinTech, Rosemont, IL, cat # 14730-1-AP, lot # 00024921), anti-NCAM (1:1000, cat # AB5032, lot # LV1487828); anti-NF-H (1:1000, cat # AB5539, lot # 2519335); anti-PERK (1:1000; Cell Signaling Technology, Danvers, MA, cat # C33E10, lot # 5); anti-PDI (1:1000; Cell Signaling Technology, Danvers, MA, cat # C81H6, lot # 2); and anti-synaptophysin (1:200; Chemicon, Temecula, CA, cat # MAB368, lot # 3388841), anti-calretinin (1:500, cat # AB5054, lot # 2465124), anti-pJNK (1:50, Cell Signaling, Danvers, MA, cat # 4668S, lot # 11), anti-S100 (1:500, DAKO, Carpinteria, CA, cat # Z031129-2, lot # 00084964). α -bungarotoxin ([α -BTX], 1:500; Invitrogen, Grand Island, NY, cat # B35451, lot # 1724058) was applied together with anti-NF-H primary antibody. Antigen retrieval was performed for PERK and PDI immunocytochemistry; sections were treated with 0.01 mol/L sodium citrate, pH 9.0, at 80°C water bath for 3 hr prior to incubation with primary antibody. After PBS washes, either fluorescent conjugated (goat AlexaFluor 488, Cy3) or biotinylated secondary antibodies (Vector Laboratories, Burlingame, CA) were used. When using biotinylated secondary antibodies, ABC Kit (Vector Labs Inc., Burlingame, CA), and DAB substrate (Vector Labs Inc., Burlingame, CA) were used for detection, as directed by the manufacturer. For pJNK immunocytochemistry was performed as previously described.¹⁹ For UCHL1/S-100 co-immunohistochemistry, a sequential protocol was

used; sections were first incubated with rabbit anti-UCHL1 primary antibody, followed by goat anti-rabbit FAB fragments (Jackson ImmunoResearch, West Grove, PA) to change the antibody species, and donkey anti-goat AlexaFluor 647. Sections were then incubated with rabbit anti-S100 (DAKO, Carpinteria, CA, cat # Z031129-2, lot # 00084964) and α -BTX conjugated with AlexaFluor 568 (1:500; Invitrogen, Grand Island, NY, cat # B35451, lot # 1724058), and S100 was detected using donkey anti-rabbit AlexaFluor 488 conjugated secondary antibody. In another set of experiments S100 primary antibody was omitted to control for cross-reactivity of secondary antibodies.

Electron microscopy

Mice were perfused with EM grade 4% PFA. Motor and sensory branch of femoral nerve were dissected out and postfixed in 2% PFA and 0.5% glutaraldehyde overnight. Tissue was then postfixed in buffered 2% OsO₄, rinsed with distilled water and stained in 1% uranyl acetate, again rinsed with distilled water, dehydrated in ascending grades of ethanol with transition fluid propylene oxide and embedded in resin mixture with Embed 812 and cured in a 60°C oven for 3 days. Tissue was mounted on resin block, and was sectioned on a Leica Ultracut UC6 ultramicrotome. 70-nm-thin sections were collected on 200 mesh copper-palladium grids. Grids were counter stained with 8% radioactive depleted uranyl acetate for 20 min. Grids were examined on FEI Tecnai Spirit G2 TEM, and digital images were captured on an FEI Eagle camera.

In vivo electrophysiological recording from motor neuron units

WT and UCHL1^{-/-} mice ($n = 3$ for postnatal day (P) 40 and P80) were anesthetized with an IP injection of pentobarbital sodium (70 mg/kg), and thereafter maintained by IV infusion of supplemental doses of pentobarbital (6 mg/kg) as needed. A tracheotomy was performed, and mice were artificially ventilated with pure oxygen (SAR-830/P ventilator; CWE, Ardmore, PA). The end tidal PCO₂ was maintained around 4% (MicroCapstar; CWE, Ardmore, PA). The heart rate was monitored, and the central temperature was kept at 38°C using an infrared heating lamp. A catheter was introduced in the external jugular vein for anesthesia supplementation and fluid infusion. All the nerves of the hindlimb were dissected and cut, except for the branches innervating the triceps surae muscle (gastrocnemius medialis and lateralis, and soleus), which were left intact, and mounted on a monopolar electrode. The distal tendon of the triceps surae was dissected free and sutured

to an isometric force transducer (BG-100, Kulite Instruments, Leonia, NJ). The length of the muscle was adjusted so that the twitch response was maximal. A pair of fine silver wires was inserted under the fascia of the triceps surae to record electromyography activity. The force and the compound muscle action potential produced by stimulation of the nerve at low frequency (0.5 Hz) and at varying intensity were recorded for off-line analysis, as previously described.²⁰

Imaging and quantification

Nikon SMZ1500 and Nikon Eclipse TE2000-E fluorescence microscopes equipped with Intensilight C-HGFI (Nikon Inc., Melville, NY) were used. Epifluorescence images were acquired using a Digital Sight (DS)-Qi1MC CCD camera (Nikon Inc.), and light images were acquired using a Ds-Fi1 camera (Nikon Inc.). Confocal images were collected using a Zeiss 510 Meta confocal microscope (Carl Zeiss Inc., Thornwood, NY).

The total number of ChAT-stained neurons were counted and averaged from at least five cervical and lumbar spinal cord sections, blinded to the genotype ($n = 4$). Statistical differences were determined by one-way analysis of variance (ANOVA) with *post hoc* Tukey's multiple comparison parametric test.

Number of total and degenerating axons in the toluidine blue stained nerve cross sections were quantified by two independent observers, blinded to the genotype ($n = 3$). Degenerating axons were defined based on their dark cytoplasmic inclusions, disintegration of their myelin sheet, and engulfment by phagocytes. Thin sections containing two entire femoral nerve branches ($n = 3$) were imaged using a 63 \times objective. Images were analyzed in Image J (<http://imagej.nih.gov/ij/>) using G-ratio calculator 1.0 plugin to calculate G ratios and axon diameters. Statistical differences were determined by unpaired *t*-test.

Soleus and EDL muscles were sectioned serially at 30 μ m. Quantifications were done on at least 100 NMJ per subject by two independent observers, blinded to the genotype ($n = 3$) at p40 and p100. Reported is percent of innervation considered as a full merge of α -BTX and anti-NF-H and percent healthy considered as the NMJ ability to maintain its pretzel-like secondary structure. Statistical differences were determined by one-way ANOVA with *post hoc* Tukey's multiple comparison parametric test.

Statistical analysis

All statistical analyses were performed using Prism software (version 6; Graphpad Software Inc., La Jolla, CA). Statistically significant differences were determined after

either one-way ANOVA with *post hoc* Tukey's multiple comparison tests or *t*-test considered. Statistically significant differences were considered at least $P < 0.05$, and values were expressed as the mean \pm SEM.

Results

Spinal motor neuron soma remain intact in the absence of UCHL1 function

UCHL1 is a neuronal protein⁶ expressed in neurons (Fig. 1A), but not the Schwann cells and myelin sheaths²¹ surrounding the motor axons (Fig. S1) in the mouse spinal cord. UCHL1 protein is detected in both the cytoplasm and the nucleus²¹ of WT spinal motor neurons (SMN) that are located in the ventral horn of the spinal cord and express ChAT (Fig. 1A). In addition, UCHL1 is present in SMN axons (Fig. 1B), which extend toward muscle targets and innervate muscle fibers at the site of neuromuscular junctions (NMJ). Motor end-plates, visualized by α -BTX staining, are innervated by SMN axons, colabeled with neurofilament-H (NF-H) and UCHL1 immunocytochemistry (Fig. 1B), further confirming presence of UCHL1 even at the site of NMJ. UCHL1 protein is thus present both in the soma and in the axon of SMN in WT mice.

UCHL1^{-/-} mice are generated by a spontaneous deletion of parts of exon 6 and the intron 6 of the *Uchl1* gene¹⁵ (Fig. 1C), resulting in the creation of a premature stop codon (denoted by "star" in Fig. 1C). UCHL1^{-/-} mice are born normal with expected Mendelian ratios, but start displaying motor defects by P40, and progress to full hindlimb paralysis (HLP) by P100,¹⁶ but can live up to P200 with assisted feeding. Heterozygous UCHL1^{+/-} mice, on the other hand, do not show any sign of motor dysfunction.

We previously studied and documented the timing and extent of motor function defects and the cellular basis of CSMN vulnerability in the absence of UCHL1 function,¹⁶ but the spinal cord component of motor neuron circuitry remained unexplored. In an effort to understand the potential role of UCHL1 on motor neuron biology, we investigated SMN health and connectivity in the UCHL1^{-/-} mice. UCHL1 protein was not present in the spinal cord of UCHL1^{-/-} mice either by western blot (Fig. 1D) or immunocytochemistry (Fig. 1E). Even though UCHL1 was expressed at high levels both in SMN soma and the axon in WT mice, it was absent from muscle fibers and UCHL1 protein was not expressed either in the muscle or in the axons in the UCHL1^{-/-} mice (Fig. 1F).

Unlike CSMN,¹⁶ SMN cell bodies were present in both the cervical and lumbar spinal cord of UCHL1^{-/-} mice

even at P200. Both Nissl staining (Fig. 2A), and ChAT immunocytochemistry (Fig. 2B) revealed lack of prominent SMN loss in the absence of UCHL1 function. The average numbers of ChAT⁺ SMN in WT and UCHL1^{-/-} mice were comparable both in the cervical (WT cervical: 55 ± 10 ; UCHL1^{-/-} cervical: 47 ± 6) and lumbar (WT lumbar: 47 ± 6 ; UCHL1^{-/-} lumbar: 49 ± 5 ; $n = 4$; Fig. 2D) sections of the spinal cord at P100 (one-way ANOVA followed by Tukey's multiple comparisons test). SMN numbers remained comparable between WT and UCHL1^{-/-} mice even at P200 (WT cervical: 54 ± 3 ; lumbar: 51 ± 4 ; UCHL1^{-/-} cervical: 44 ± 5 ; lumbar: 47 ± 6 ; $n = 4$; one-way ANOVA followed by Tukey's multiple comparisons test; Fig. 2D), revealing a lack of prominent SMN degeneration in the absence of UCHL1 function.

These striking differences between CSMN and SMN, and lack of prominent SMN loss suggested SMN might not be as vulnerable as CSMN are in the absence of UCHL1 function. Since mice displayed hindlimb paralysis, we focused our attention to the lumbar section of the spinal cord, and because CSMN displayed apical dendrite degeneration and spine loss in the absence of UCHL1,¹⁶ we decided to investigate whether neurons in spinal cord suffered a similar loss of synaptic input. Synaptophysin is used to mark locations of synapses on ChAT⁺ SMN (Fig. 2C) and calretinin⁺ interneurons (Fig. S2) in WT and UCHL1^{-/-} mice at P200. The numbers of synaptophysin⁺ puncta per 10 μ m of SMN soma length were comparable between WT (lumbar: 1.3 ± 0.3 ; $n = 4$) and UCHL1^{-/-} mice (lumbar: 1.4 ± 0.1 ; $n = 3$, two-tailed unpaired *t*-test; Fig. 2E). Similar to SMN, there was no significant difference in the numbers of synaptophysin⁺ puncta per 10 μ m of interneuron (calretinin⁺) soma length in WT (lumbar: 1.4 ± 0.1 $n = 2$) and UCHL1^{-/-} mice (lumbar: 1.3 ± 0.2 ; $n = 3$, two-tailed unpaired *t*-test). In addition, unlike CSMN,¹⁶ SMN did not display any signs of increased ER stress. The expression of PERK, and PDI, two prominent markers of increased ER stress²² were comparable between WT and UCHL1^{-/-} SMN (Fig. 2F; Fig. S3). Our results show that the average number of synapses on SMN soma was not altered in UCHL1^{-/-} mice suggesting that SMN and CSMN were affected differently in the absence of UCHL1 function. Since SMN did not display major cell loss in UCHL1^{-/-} mice, which develop motor dysfunction, we reasoned presence of potential defects in sensory input.

Axonal degeneration is restricted to motor axons

Sensory input is one of the major modulators of motor function in the spinal cord. Some of the phenotype that

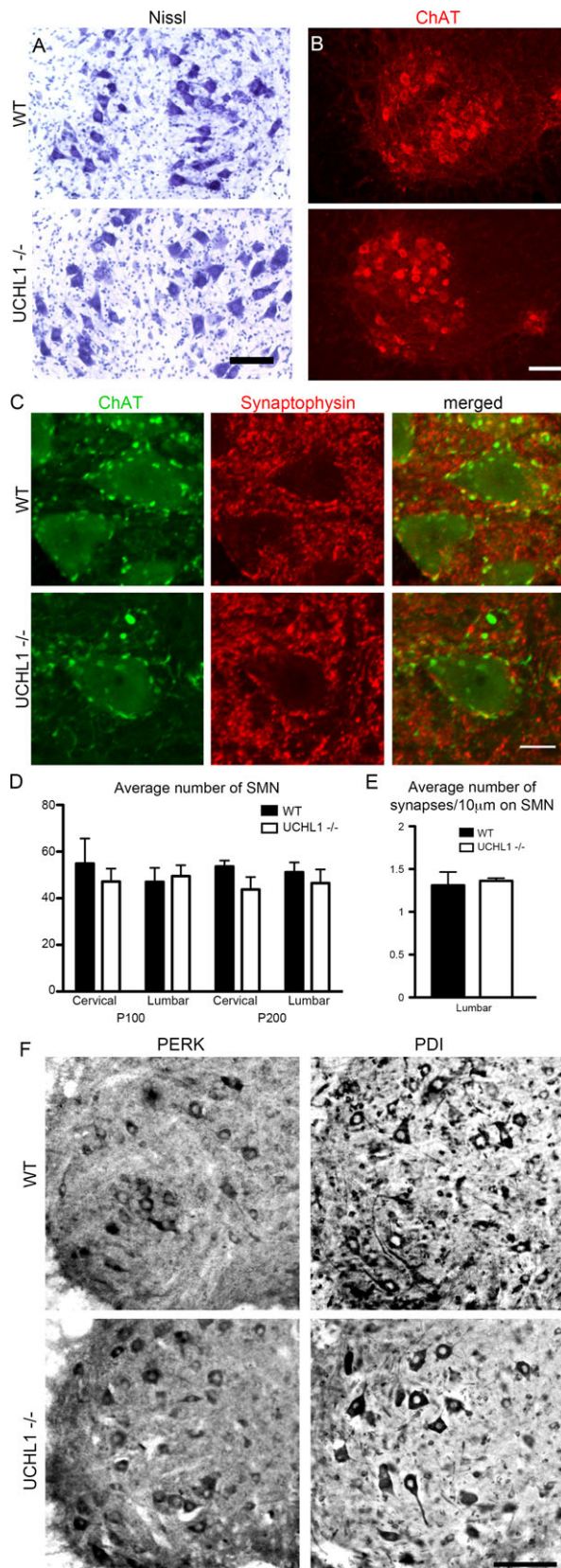


Figure 2. SMN are resistant to degeneration in the absence of UCHL1 function. Nissl staining (A), and ChAT immunocytochemistry (B) reveal conservation of SMN soma in the spinal cord of UCHL1^{-/-} mice, even at P200. (C) Representative images of both WT and UCHL1^{-/-} SMN with synaptophysin+ puncta present along their cell membrane at P200. (D) Bar graph distribution of average number of SMN (ChAT+ neurons) in WT and UCHL1^{-/-} mice at P100 and P200. (E) Bar graph distribution of average number of synapses (synaptophysin+ puncta) per 10 μ m of cell membrane of WT and UCHL1^{-/-} SMN located in lumbar spinal cord. (F) There is no sign of increased endoplasmic reticulum-stress in UCHL1^{-/-} SMN at P200, as depicted by comparable levels of PERK and PDI expression in WT and UCHL1^{-/-} SMN. Scale bars: A, B, and F = 100 μ m, C = 20 μ m.

is observed as “motor dysfunction” in mice could indeed stem from sensory input defects. To investigate the potential contribution of the sensory system to the observed motor function deficits, motor and sensory branches of the femoral nerve and the ventral root were examined (Fig. 3A), and the extent of axonal degeneration was quantified. The total numbers of either axons in sensory branch of the femoral nerve (WT: 865.7 ± 11.8 , $n = 3$; UCHL1^{-/-}: 897 ± 17.2 , $n = 3$; Fig. 3B and E) or proximal motor axons at the level of ventral root (WT: 951 ± 89 , $n = 3$; UCHL1^{-/-}: 1004 ± 114 , $n = 5$; Fig. 3C and G) were comparable between WT and UCHL1^{-/-} mice even at P200. In addition, no signs of degeneration were detected in the femoral nerve sensory branch (WT: $9 \pm 3\%$, $n = 3$; UCHL1^{-/-}: $9.4 \pm 0.1\%$, $n = 4$; Fig. 3F) and in the ventral root (WT: $13.5\% \pm 1.3$, $n = 3$; UCHL1^{-/-}: $16 \pm 0.7\%$, $n = 5$; Fig. 3H). Even though the total numbers of distal motor axons at the level of femoral nerve (Fig. 3D) were comparable between WT and UCHL1^{-/-} mice (WT: 459 ± 13 , $n = 3$; UCHL1^{-/-}: 448 ± 14 , $n = 3$, Fig. 3I), there was significant axonal degeneration only in the motor branch of the femoral nerve in UCHL1^{-/-} mice (WT: $6 \pm 2\%$, $n = 3$; UCHL1^{-/-}: $22 \pm 3\%$, $n = 3$; $P = 0.0146$, two-tailed unpaired t -test; Fig. 3J). To further assess selective degeneration in the motor branch of the femoral nerve, we measured the G-ratio and axon diameters. G-ratio is a measure of myelin thickness that is proportional to the size of the fiber based on the inner area/total area of the axon fiber. G-ratio is significantly reduced in the motor branch of the femoral nerve (WT, 0.674 ± 0.009 , $n = 3$; UCHL1^{-/-}, 0.607 ± 0.008 , $n = 3$; $P = 0.0048$, two-tailed unpaired t -test; Fig. 3K). As hypermyelination (decreased G-ratio) could result either due to increased thickness of myelin layer or pathological shrinkage of the axonal caliber,²³ we next evaluated the axon size distribution of the femoral motor axons. Analysis of axonal diameter also revealed a decline especially in the percentage of the large axons with a diameter of $>7.5 \mu\text{m}$ ($3\text{--}3.5 \mu\text{m}$ range: WT, $7.7 \pm 0.8 \mu\text{m}$; UCHL1^{-/-}, $12.7 \pm 1.3 \mu\text{m}$; $P = 0.0271$,

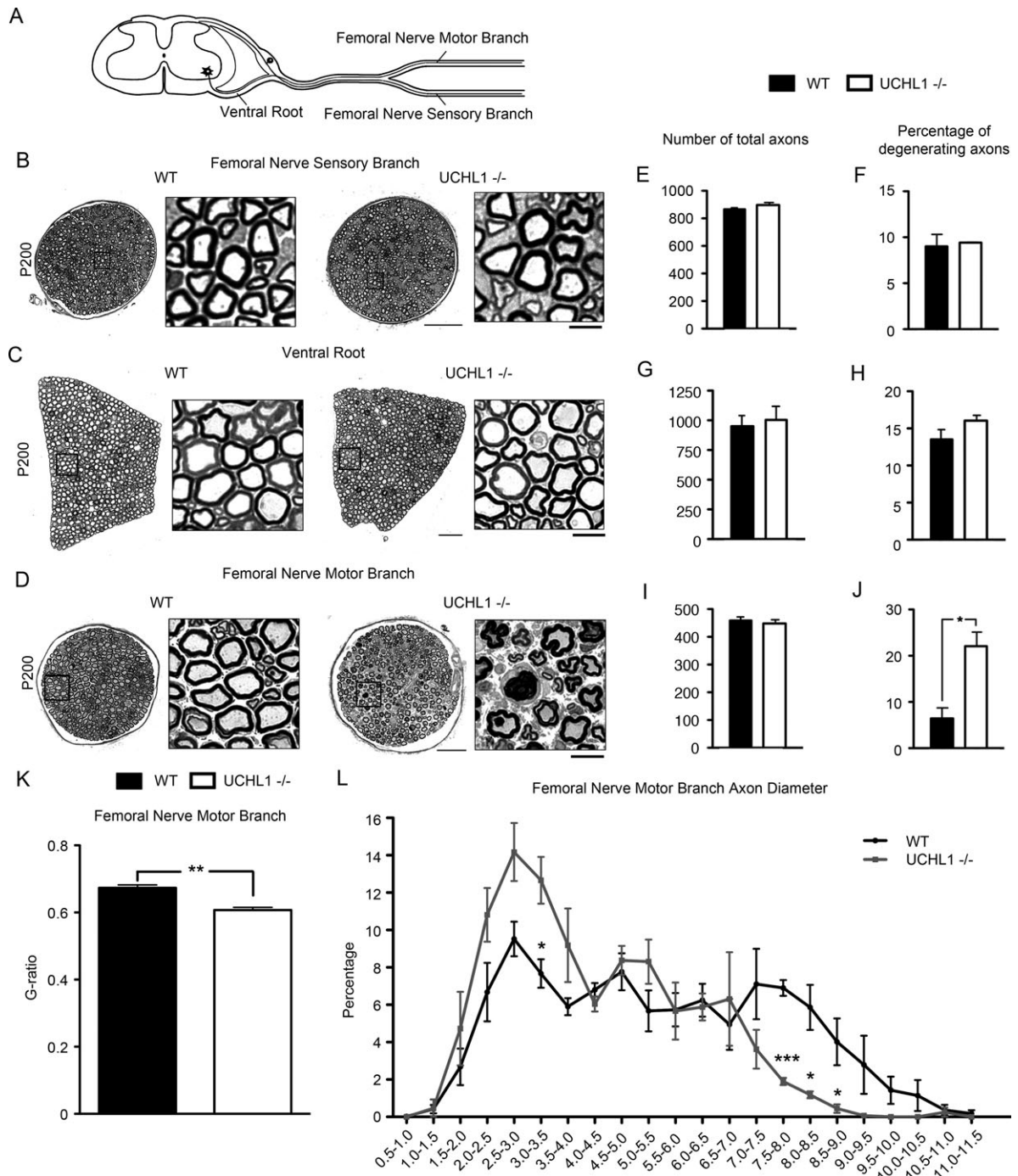


Figure 3. There is selective, progressive and directional motor axon degeneration in the absence of UCHL1^{-/-} function. (A) A schematic diagram showing a cross section of the spinal cord with both sensory and motor axons. SMN axons are present in the motor branch of the femoral nerve and in the ventral root, whereas the sensory axons of the DRG are present in the sensory branch of the femoral nerve. Toluidine blue staining of the motor branch of the femoral nerve (B), ventral root (C), and the sensory branch of the femoral nerve (D) at P200 in WT and UCHL1^{-/-} mice. Boxed areas are enlarged to the side. (E–J) Average number of total axons and the average percentage of degenerating axons in the motor branch of the femoral nerve (E–F), ventral root (G–H), and the sensory branch of the femoral nerve (I–J). (K) G-ratio quantification of the femoral nerve motor branch axons. (L) Distribution of femoral nerve motor branch axons based on axon diameter. Scale bars: B, C, and D = 100 μm; B and C inset = 20 μm; D inset = 10 μm. **P* < 0.05, ***P* < 0.01, ****P* < 0.001.

two-tailed unpaired *t*-test; 7.5–8 μm range: WT, $6.9 \pm 0.4 \mu\text{m}$; UCHL1^{-/-}, $1.9 \pm 0.2 \mu\text{m}$; $P = 0.0004$, two-tailed unpaired *t*-test; 8–8.5 μm range: WT, $5.9 \pm 1.2 \mu\text{m}$; UCHL1^{-/-}, $1.2 \pm 0.2 \mu\text{m}$; $P = 0.0186$, two-tailed unpaired *t*-test; 8.5–9 μm range: WT, $4 \pm 1.2 \mu\text{m}$; UCHL1^{-/-}, $0.4 \pm 0.2 \mu\text{m}$; $P = 0.0484$, two-tailed unpaired *t*-test; $n = 3$, WT: 1908 axons, $n = 3$. UCHL1^{-/-}: 1160 axons, Fig. 3L).

EM analysis revealed that cytoplasmic composition of both motor and sensory branch of the femoral nerve were comparable between WT and UCHL1^{-/-} mice (Fig. 4A and G). The orientation of neurofilaments and microtubules were normal, and mitochondria were present (Fig. 4B–D, F and H). However, axons in the motor branch (Fig. 4B–F) showed severe shrinkage (atrophy) of the cytoplasmic area. In some axons the atrophy of the cytoplasmic area was mild (Fig. 4C), whereas in others, especially in larger caliber nerves, it was massive, leading to the collapse of myelin sheath and a lobular appearance (Fig. 4B, D and E). In few cases, the axons were totally absent from the myelin sheath (Fig. 4E) which folds onto itself. In final stage the axon was scavenged by macrophages (Fig. 4F). Altogether, these results demonstrate selective axonal defects only in the motor, but not in the sensory axon, which rule out the possibility that the observed motor dysfunction is primarily related to sensory abnormalities. Moreover, axonopathy is observed only in the distal motor axons at the level of femoral nerve, but not proximal to SMN cell bodies at the level of the ventral root, suggesting the presence of a progressive and directional axonal degeneration from periphery toward soma in the absence of UCHL1 function. This striking selective motor, but not sensory, axonopathy suggested potential defects at NMJ.

UCHL1 is required for maintaining the structure of the NMJ

Even though UCHL1^{-/-} mice grow with comparable size and rate with their littermates, there is progressive muscle atrophy only at later ages (Fig. S4A). Because UCHL1 is not expressed in the WT muscle (Fig. 1F), and axonal degeneration is detected only in the motor axons, muscle atrophy is thought to be a consequence of NMJ defects.^{12,24} Visualization of the motor end-plates with α -BTX and the presynaptic innervation by NF-H immunocytochemistry revealed profound structural defects in two major muscle groups only in UCHL1^{-/-} mice (Fig. 5A–B). The EDL muscle, which is mainly innervated by fast-twitch SMN revealed profound NMJ defects in the absence of UCHL1 function (P40 WT: $82 \pm 4.5\%$ innervated, $97.7 \pm 1.3\%$ healthy, $n = 3$; P100 WT: $65.3 \pm 10.5\%$ innervated, $97 \pm 2.1\%$ healthy, $n = 3$; P40

UCHL1^{-/-} mice: $84 \pm 3.1\%$ innervated, $94.7 \pm 0.9\%$ healthy, $n = 3$; P100 UCHL1^{-/-} mice: $30.3 \pm 4.2\%$ innervated, $54.3 \pm 14.8\%$ healthy, $n = 3$; EDL innervation: P40 UCHL1^{-/-} versus P100 UCHL1^{-/-} adjusted P value = 0.0014, P100 WT versus P100 UCHL1^{-/-} adjusted P value = 0.018; E.D.L. health: P40 UCHL1^{-/-} versus P100 UCHL1^{-/-} adjusted P value = 0.022, P100 WT versus UCHL1^{-/-} adjusted P value = 0.0165; one-way ANOVA followed by Tukey's multiple comparisons test; Fig. 5C,E and F). Likewise, soleus muscle, which is mainly innervated by slow-twitch SMN displayed major NMJ defects (P40 WT: $97 \pm 2.5\%$ innervated, $89.3 \pm 5.2\%$ healthy, $n = 3$; P100 WT: $81 \pm 6.6\%$ innervated, $93 \pm 1\%$ healthy, $n = 3$; P40 UCHL1^{-/-} mice: $79.7 \pm 7.9\%$ innervated, $86.7 \pm 2.9\%$ healthy, $n = 3$; P100 UCHL1^{-/-} mice: $39.3 \pm 6.8\%$ innervated, $48.3 \pm 6.8\%$ healthy, $n = 3$; soleus innervation: P40 UCHL1^{-/-} versus P100 UCHL1^{-/-} adjusted P value = 0.0085, P100 WT versus P100 UCHL1^{-/-} adjusted P value = 0.007; soleus health; P40 UCHL1^{-/-} versus P100 UCHL1^{-/-} adjusted P value = 0.0016, P100 WT versus P100 UCHL1^{-/-} adjusted P value = 0.0006, one-way ANOVA followed by Tukey's multiple comparisons test; Fig. 5D,G and H). In addition, denervated muscle fibers were observed in the gastrocnemius muscle from UCHL1^{-/-} mice by nonspecific esterase (NSE) staining and neural cell adhesion molecule (NCAM) immunocytochemistry (Fig. S4B and D). Similar NMJ defects were reported in ubiquitin-specific protease 14 (Usp14) deficient ataxia (*ax^J*) mice, due to an increase in c-Jun N-terminal kinase (JNK) phosphorylation.¹⁹ Therefore, we decided to investigate JNK and phospho JNK (pJNK) levels in UCHL1^{-/-} mice. There was an increase in pJNK levels in the UCHL1^{-/-} spinal cord lysates compared to WT at P100 (an increase between 25 and 62% was observed in three independent experiments; Fig. S5A–B). pJNK was also detected at the NMJ of WT mouse EDL muscle at P200 (Fig. S5C) suggesting their possible involvement, although more experiments are needed to investigate this further. These qualitative and quantitative findings in different muscle groups confirmed that UCHL1 was not primarily important for a subset of SMN population, but rather was a key molecule required by a broad range of SMN to maintain a functional NMJ, potentially through a mechanism involving JNK pathway.

Transmission of excitation to the muscle fibers is less efficient in UCHL1^{-/-} mice

To investigate how these expressional analyses correlate with *in vivo* motor function defects, we studied the electrical activity of muscle fibers in intact WT and UCHL1^{-/-} mice at P40 and P80, using a novel *in vivo*

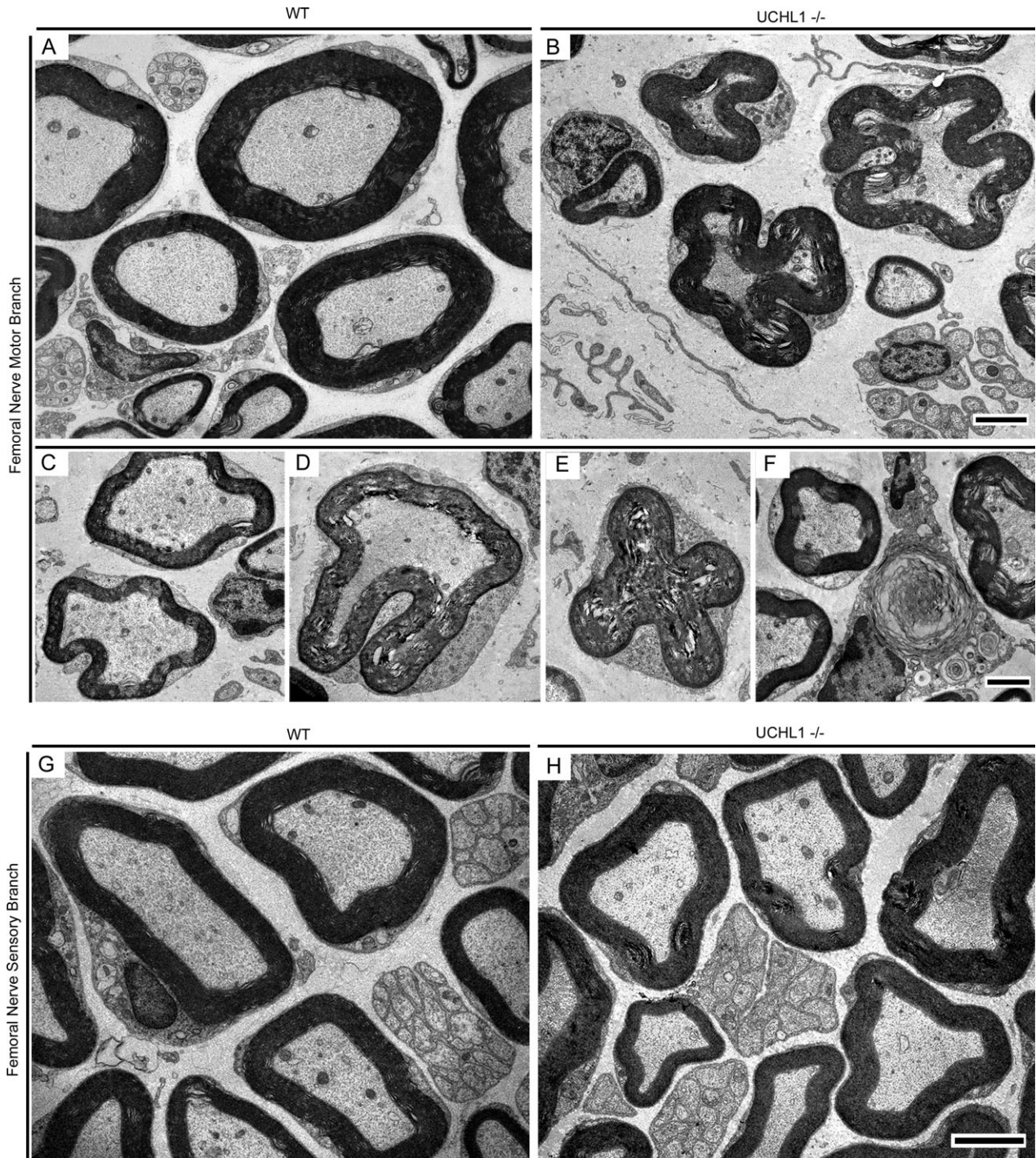


Figure 4. Axon fibers in the motor branch of femoral nerve display selective axonal degeneration. (A) A representative cross section image of axons within the motor branch of the femoral nerve in WT mice. Axons with different sizes, and the intact myelin sheath around them is observed with electron microscope. (B) A representative cross-sectional image of axons within the motor branch of the femoral nerve in UCHL1^{-/-} mice. Axons fibers with various degrees of degeneration are present. (C-E) Representative images displaying stages of axonal defects. (C) Initial stage of axon fiber collapse, (D) intermediary stage showing invagination of myelin sheath, and (E) a completely collapsed axon fiber. (F) An example of completely degenerated axon fiber being scavenged by macrophage. (G-H) Representative cross-sectional electron micrographs of sensory branch of the femoral nerve in WT (G) and UCHL1^{-/-} (H) mice appear comparable, and both are devoid of major axonal defects. Scale bar: 2 μ m.

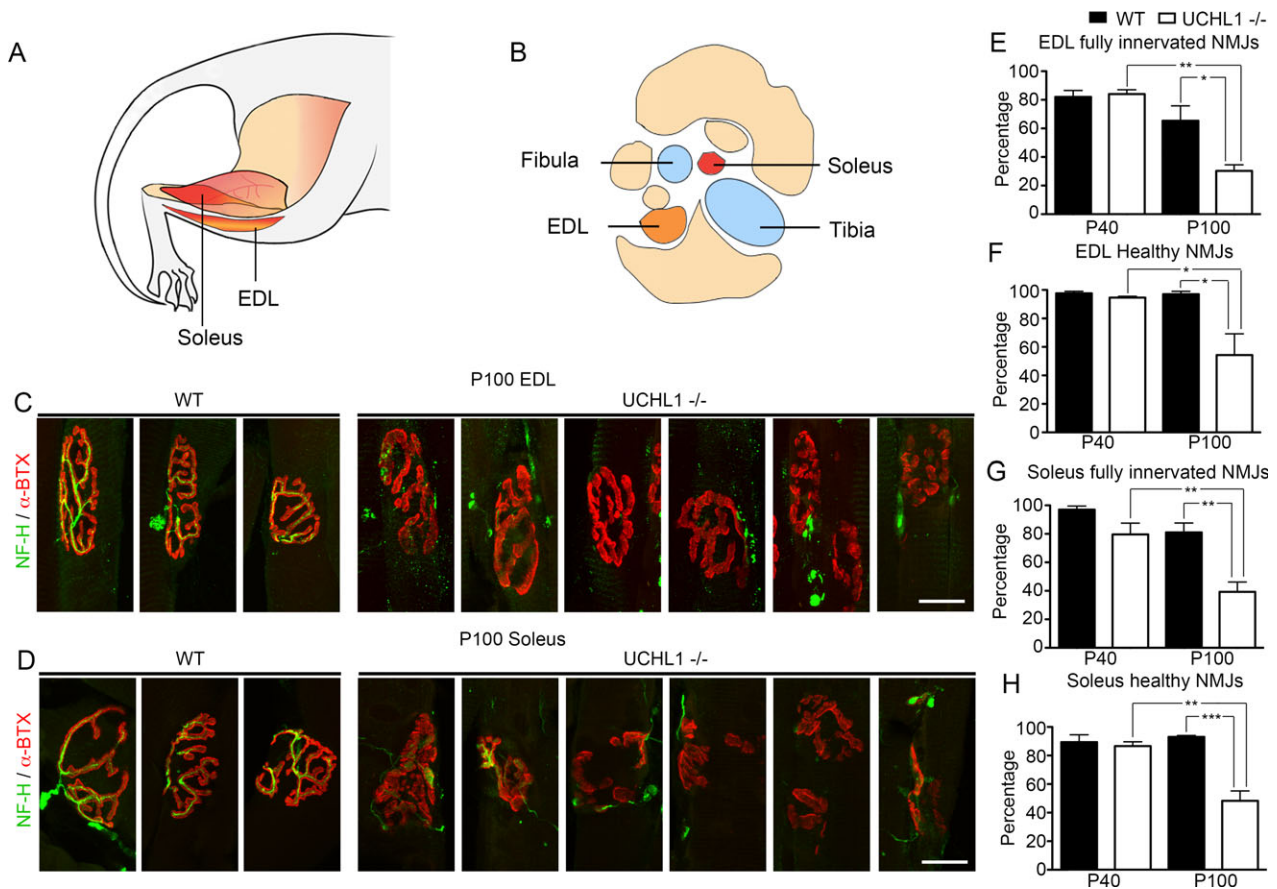


Figure 5. UCHL1 is required for the maintenance of NMJ in different muscle groups. (A) A schematic drawing of the hindlimb depicting the location of soleus and EDL muscles. (B) Schematic drawing of the cross section of the hindlimb depicting the relative location of soleus and EDL to other different muscle groups and bones fibula and tibia. (C) Representative images of NMJ from the EDL muscle of WT (3 left panels) and UCHL1^{-/-} mice (6 right panels) at P100. SMN axons are visualized by NF-H (green) and postsynaptic acetylcholine receptors are visualized by α -BTX (red). WT NMJ are intact with overlapping green and red signal, whereas the NMJ in UCHL1^{-/-} mice display many different examples of denervation and disintegration. (D) Representative images of NMJ from the soleus muscle of WT (3 left panels) and UCHL1^{-/-} mice (6 right panels) at P100. SMN axons are visualized by NF-H (green) and postsynaptic acetylcholine receptors are visualized by α -BTX (red). WT NMJ are intact, whereas the NMJ in UCHL1^{-/-} mice display many different examples of denervation and disintegration. (E) Bar graph representation of percent distribution of fully innervated NMJ in the EDL muscle of WT and UCHL1^{-/-} mice at P40 and P100. (F) Bar graph representation of percent distribution of healthy NMJ in the EDL muscle of WT and UCHL1^{-/-} mice at P40 and P100. (G) Bar graph representation of percent distribution of fully innervated NMJ in the soleus muscle of WT and UCHL1^{-/-} mice at P40 and P100. (H) Bar graph representation of percent distribution of healthy NMJ in the soleus muscle of WT and UCHL1^{-/-} mice at P40 and P100. Scale bar = 20 μ m. * P < 0.05, ** P < 0.01, *** P < 0.001. BTX, bungarotoxin; EDL, extensor digitorum longus.

electrophysiology approach.²⁰ The nerves innervating the triceps surae (TS) muscle of WT and UCHL1^{-/-} mice were stimulated and the electrical activity of muscle fibers (i.e., compound muscle action potential [CMAP]), as well as the force generated by the muscle in response to repeated low-frequency nerve stimulation were recorded (Fig. 6A). There was no difference between the delay of the CMAPs and the onset of force. The maximum force produced by the TS muscle in response to a single stimulus in the WT and UCHL1^{-/-} mice was detected with high precision and indicated a lower force for UCHL1^{-/-} than WT mice at P40 and P80 (Fig. 6B-C). To account

for the muscle atrophy observed in UCHL1^{-/-} mice (Fig. S4), we normalized the force by the wet weight of the TS muscle. The normalized force values were comparable between WT and UCHL1^{-/-} mice at P40, but significantly lower in UCHL1^{-/-} mice at P80 (Fig. 6B-C). In WT mice, the electrical activity of muscle was very consistent from stimulation to stimulation, and lasted for only a short period of time, displaying only a few peaks at P40 and P80. However, the profile of CMAPs was very different in UCHL1^{-/-} mice, with the appearance of a high latency activity that could last for several tens of milliseconds (Fig. 6C). Furthermore, CMAPs showed

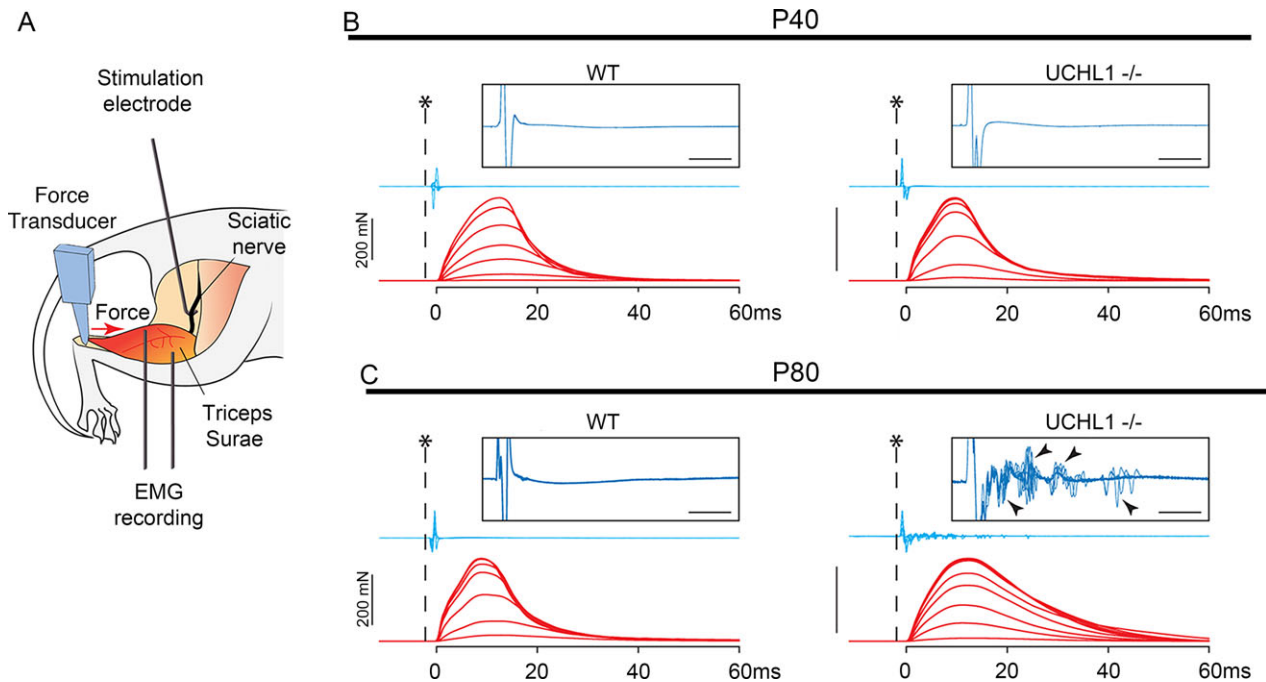


Figure 6. There is early motor unit dysfunction in *UCHL1*^{-/-} mice. (A) Schematic drawing of electromyography recording from triceps surae muscle in intact animal. Force response and muscle fiber electrical activity in WT and *UCHL1*^{-/-} mice show no differences at P40 (B), but delayed electrical activity (arrowheads) is observed in the *UCHL1*^{-/-} mice at P80 (C). The electrical stimulation of the sciatic nerve (asterisks and dashed line) elicited an electrical response in the triceps surae muscle (CMAPs, blue traces) followed by a twitch (red trace). The responses to increasing stimulation intensity from motor threshold to maximal response are shown in each quadrant. Inserts indicate magnification of the CMAPs elicited by the highest intensity stimulation (amplitude truncated, scale bar 5 msec in each insert). 6–10 sweeps are superimposed in each insert to illustrate the variability in the response. Scale bars: B and C = 200 mN. CMAP, compound muscle action potential.

numerous jitter from stimulation to stimulation only in *UCHL1*^{-/-} mice at P80 ($n = 3$). These *in vivo* recordings further revealed the importance of *UCHL1* function not only for the formation, but also for the maintenance of NMJ function in a broad range of muscle groups. In the absence of *UCHL1*, there is gradual defect at the site of SMN and muscle interaction, which progressively results into directional motor axon degeneration that extends from NMJ to SMN soma. However, unlike CSMN, SMN cell bodies not vastly affected and maintain their integrity even at later stages.

Discussion

To date many different aspects of *UCHL1* function and its involvement in a broad perspective of cellular events have been studied,^{6,13} and yet its distinct role and importance is not fully understood. Even though *UCHL1* is a unique deubiquitinating enzyme (DUB) with abilities to add and remove ubiquitin from a protein, and is involved in many different cellular events, patients with mutations in their *UCHL1* gene display early neurodegeneration and motor dysfunction.^{1,2,25} Motor neuron diseases are one of

the most complex diseases of the nervous system, not only because the motor neuron circuitry requires proper function and connectivity of many different neuron populations, but also because maintaining homeostasis of the system is a demanding act.

Patients with defective *UCHL1* and that display spasticity in the legs and problems with locomotion and voluntary movement.^{1,2,25} Similarly, the *UCHL1*^{-/-} mice have poor rotarod performance, decreased grip strength and abnormal gait, with complete hindlimb paralysis by P100, which is relatively early when compared with other mouse models for motor neuron diseases. We previously found that in the absence of *UCHL1*, CSMN display very early and profound degeneration with spine loss and disintegration of apical dendrites,¹⁶ suggesting a potential role for maintenance of spines and neuronal connectivity.

Selective axonal degeneration in the same mouse is remarkable. In many diseases the motor and the sensory systems are affected either to a different degree or pattern. Axonopathy of distal ends of long central nervous system axons, especially upper motor neurons defines hereditary spastic paraplegia (HSP) syndrome. However, peripheral neuropathy has been described as either a rare or

common feature in more than a dozen genetic types of HSP.²⁶ In our study, we find distal motor neuropathy but not motor-sensory neuropathy, in support of our observations, some HSP subjects exhibit strictly distal motor neuropathy.²⁷ Axon length-dependent motor neuropathy is also a common feature of distal hereditary motor neuropathies (dHMN), and many forms of dHMN also have a significant upper motor neuron component.²⁸ Delineating the sensory versus motor system defects in the same model system is rather complicated and challenging, and yet we found that in the absence of UCHL1 function, it is mainly the motor neuron circuitry that is affected, and the sensory axons remain healthy.

NMJ is a specialized synapse and UCHL1 was previously reported to be important for the maintenance of the structure and function of not only the NMJ,¹² but also hippocampal neuron synapses.^{15,29} For example, inhibition of UCHL1 activity increases hippocampal neurons spine size, while decreasing spine density.⁴ Reduced hippocampal CA1 LTP was reported in another mouse model of UCHL1, accompanied by reduction in memory in passive avoidance learning and exploratory behavior.²⁹ Inhibition of UCHL1 function by LDN reduced basal synaptic transmission and LTP in hippocampal slices.³⁰ Moreover, exogenous UCHL1 rescues β -amyloid-induced decreases in synaptic function (LTP).³⁰ These studies suggest that UCHL1 plays a broad role in maintaining synaptic structure and functional connectivity in many different neuron types in the cortex.

Interestingly, lack of UCHL1 function also resulted in increased ER stress mainly in CSMN as they failed to maintain their homeostasis and became vulnerable to degeneration. Even though ER stress was also increased in other cortical neurons, they were able to cope with the stress, whereas CSMN failed. However, Guanabenz, which alleviates ER stress,³¹ improved CSMN survival *in vitro*. So even though a broad spectrum of neurons required UCHL1 function for spine health and connectivity, it seem to play a unique role for CSMN, especially within the context of ER stress. This is no surprise as there is a direct relationship between problems with the UPS and increased ER stress.^{32,33}

In contrast to the profound and early CSMN degeneration, SMN remained intact in the spinal cord with no obvious cell loss in the same mice that lacked all UCHL1 function. This is not only interesting, but also is very informative. UCHL1 seem to play distinct roles in upper and lower motor neuron populations. CSMN could be more dependent on UCHL1 function for retaining its cellular cytoarchitecture, maintaining the integrity of its apical dendrite and the spine health, as well as controlling or maintaining ER stress at manageable levels, whereas, SMN may require UCHL1 function for other cellular events.

Unlike CSMN, SMN display no increase in ER stress in the absence of UCHL1 function, suggesting that UCHL1 is not as critically important for SMN, as it is for CSMN for managing ER stress. Different from CSMN, however, SMN display major axonal degeneration phenotype in the UCHL1^{-/-} mice. AAV-mediated anterograde transduction of CSMN revealed lack of corticospinal tract axon defects in the absence of UCHL1 function and ruled out the possibility of a “dieback” mechanism for progressive CSMN degeneration. However, in the absence of UCHL1, there was indeed a “dieback” phenomenon for SMN axon fibers, which showed defects in the NMJ, in the axon bundles of motor branch of the femoral nerve, but not at the site of ventral root. Interestingly, CST axons did not degenerate before CSMN, and the presence of directional and progressive axonal degeneration was specific to the motor, and not to the sensory axons in the femoral nerve.

Previous studies documented NMJ defects in the absence of UCHL1 function,^{12,24} however, role of UCHL1 function on the health and stability of SMN remained elusive. In this study we began to elucidate a unique role for UCHL1 function in the lower motor neuron circuitry as revealed by denervated and unhealthy NMJ in the EDL and soleus muscles, which are two important muscle groups in the leg that are the site of disease initiation in some patients, and that are primarily innervated by different types of SMN. By investigating these two different muscle groups, we studied whether NMJ defects were more restricted to a subgroup of SMN population, but found a rather broad defect in both muscle groups. *In vivo* electrophysiological recordings from intact and alive mice further revealed motor unit defects especially in the hindlimb of UCHL1^{-/-} mice. NMJ defects are the primary pathogenic event in ALS patients³⁴ as well as the hSOD1^{G93A} ALS mouse model.³⁵ We now show, UCHL1^{-/-} mice display severe HLP, muscular atrophy, accompanied by partial/complete denervation of the NMJ, and postsynaptic fragmentation.

UCHL1 is important for regulating free ubiquitin levels in neurons,^{1,4} and our data demonstrates its absence leads to NMJ denervation. Interestingly, another DUB, Usp14, which removes ubiquitin from proteosomal substrates to maintain intracellular free ubiquitin levels seems to have a very similar function. *ax^J* ataxia mice, which have a spontaneous deletion of the Usp14 gene have neuromuscular problems where NMJ undergo structural degeneration.¹⁹ Usp14 deficiency leads to an increase in K63-linked ubiquitination of mixed lineage kinase 3 (MLK3), which in turn leads to an increase in JNK phosphorylation. Our data demonstrates a similar increase in pJNK levels, suggesting a common mechanism for the importance of UPS system and ubiquitin homeostasis for

maintenance of proper NMJ structure and function. Moreover, in a mouse model of Huntington's Disease, mutant huntingtin protein contributed to selective vulnerability of affected neuron populations by inhibiting fast axonal transport through increased JNK activity.³⁶ Since CSMN and SMN are affected differently in the absence of UCHL1, it is potentially possible that alterations in the regulation of different JNK substrates in the two cell types might explain the different pathologies observed.

Despite severe NMJ defects and progressive axonal degeneration, there is very limited cellular pathology and SMN remain intact in the spinal cord, even by P200. Since we are accustomed to define pathology with cell loss, this is rather interesting. Building evidence suggest, however, that pathology is most correlated with loss of function, and even in the absence of cell loss there could be severe pathology.

In an attempt to study and understand complex diseases, we suggest to shift our attention from genes, but focus more on circuitries as well as functional defects within different components of affected circuitries in diseases. Here, we find that UCHL1 function is primarily important for the motor neuron circuitry. Even though CSMN and SMN need UCHL1 function for different cellular events, in its absence they both are affected and the whole motor circuitry becomes dysfunctional. This may in part explain why patients with mutations in their UCHL1 gene display early degeneration and motor defects.

Acknowledgments

This work was supported by grants from NIH-R01NS085161-01 (P.H.O.), Les Turner ALS Foundation, Wenske Foundation (P.H.O.), P30 NS054850-01A1 (C.J.H.); R01NS060926 and MDA 255785 (C.J.D.) NIH (5T32AG020506-09 M.A.D. Postdoctoral Training; B.G.), and ALSA Safenowitz fellowship (J.H.J. and M.M.), by the Northwestern University Mouse Histology and Phenotyping Laboratory and a Cancer Center Support Grant (NCI CA060553) and Northwestern University's Center for Advanced Microscopy and a Cancer Center Support Grant (NCI CA060553). We thank Dr. Marco Martina with analysis of electron microscopy results, and overall discussion of the manuscript. We thank Nabil A. Khan, William D. Weber, Michael W. Tu, Carolyn G. Brooks, and Amiko K.B. Lagrimas for their help with histochemistry and imaging.

Author Contributions

B.G., J.H.J., M.M., C.J.D., C.J.H., and P.H.O. designed this study; B.G., J.H.J., M.C.S., M.J.S., M. M., M. G., J. L.

K., G. S., C. J. D., and P.H.O. conducted experiments; G.A.C. shared UCHL1^{-/-} mice; all authors collected and analyzed data; and B.G., J.H.J., M. C. S., and P.H.O. wrote the manuscript.

Conflict of Interest

The sponsor had no role in the design and conduct of the study; collection, management, analysis, and interpretation of the data; preparation, review, or approval of the manuscript; and decision to submit the manuscript for publication.

References

1. Leroy E, Boyer R, Auburger G, et al. The ubiquitin pathway in Parkinson's disease. *Nature* 1998;395:451–452.
2. Bilguvar K, Tyagi NK, Ozkara C, et al. Recessive loss of function of the neuronal ubiquitin hydrolase UCHL1 leads to early-onset progressive neurodegeneration. *Proc Natl Acad Sci USA* 2013;110:3489–3494.
3. Osaka H, Wang YL, Takada K, et al. Ubiquitin carboxy-terminal hydrolase L1 binds to and stabilizes monoubiquitin in neuron. *Hum Mol Genet* 2003;12:1945–1958.
4. Cartier AE, Djakovic SN, Salehi A, et al. Regulation of synaptic structure by ubiquitin C-terminal hydrolase L1. *J Neurosci* 2009;29:7857–7868.
5. Liu Y, Fallon L, Lashuel HA, et al. The UCH-L1 gene encodes two opposing enzymatic activities that affect alpha-synuclein degradation and Parkinson's disease susceptibility. *Cell* 2002;111:209–218.
6. Day IN, Thompson RJ. UCHL1 (PGP 9.5): neuronal biomarker and ubiquitin system protein. *Prog Neurobiol* 2010;90:327–362.
7. Deng HX, Chen W, Hong ST, et al. Mutations in UBQLN2 cause dominant X-linked juvenile and adult-onset ALS and ALS/dementia. *Nature* 2011;477:211–215.
8. Johnson JO, Mandrioli J, Benatar M, et al. Exome sequencing reveals VCP mutations as a cause of familial ALS. *Neuron* 2010;68:857–864.
9. Nishimura AL, Mitne-Neto M, Silva HC, et al. A mutation in the vesicle-trafficking protein VAPB causes late-onset spinal muscular atrophy and amyotrophic lateral sclerosis. *Am J Hum Genet* 2004;75:822–831.
10. Petrucelli L, Dawson TM. Mechanism of neurodegenerative disease: role of the ubiquitin proteasome system. *Ann Med* 2004;36:315–320.
11. Rubino E, Rainero I, Chio A, et al. SQSTM1 mutations in frontotemporal lobar degeneration and amyotrophic lateral sclerosis. *Neurology* 2012;79:1556–1562.
12. Chen F, Sugiura Y, Myers KG, et al. Ubiquitin carboxyl-terminal hydrolase L1 is required for maintaining the structure and function of the neuromuscular junction. *Proc Natl Acad Sci USA* 2010;107:1636–1641.

13. Jara JH, Frank DD, Ozdinler PH. Could dysregulation of UPS be a common underlying mechanism for cancer and neurodegeneration? Lessons from UCHL1. *Cell Biochem Biophys* 2013;67:45–53.
14. Saigoh K, Wang YL, Suh JG, et al. Intragenic deletion in the gene encoding ubiquitin carboxy-terminal hydrolase in gad mice. *Nat Genet* 1999;23:47–51.
15. Walters BJ, Campbell SL, Chen PC, et al. Differential effects of Usp14 and Uch-L1 on the ubiquitin proteasome system and synaptic activity. *Mol Cell Neurosci* 2008;39:539–548.
16. Jara JH, Genc B, Cox GA, et al. Corticospinal Motor Neurons Are Susceptible to Increased ER Stress and Display Profound Degeneration in the Absence of UCHL1 Function. *Cereb Cortex* 2015;25:4259–4272.
17. Gurney ME, Pu H, Chiu AY, et al. Motor neuron degeneration in mice that express a human Cu Zn superoxide dismutase mutation. *Science* 1994;264:1772–1775.
18. Gogliotti RG, Lutz C, Jorgensen M, et al. Characterization of a commonly used mouse model of SMA reveals increased seizure susceptibility and heightened fear response in FVB/N mice. *Neurobiol Dis* 2011;43:142–151.
19. Vaden JH, Bhattacharyya BJ, Chen PC, et al. Ubiquitin-specific protease 14 regulates c-Jun N-terminal kinase signaling at the neuromuscular junction. *Mol Neurodegener* 2015;10:3.
20. Manuel M, Heckman CJ. Adult mouse motor units develop almost all of their force in the subprimary range: a new all-or-none strategy for force recruitment? *J Neurosci* 2011;31:15188–15194.
21. Wilson PO, Barber PC, Hamid QA, et al. The immunolocalization of protein gene product 9.5 using rabbit polyclonal and mouse monoclonal antibodies. *Br J Exp Pathol* 1988;69:91–104.
22. Walter P, Ron D. The unfolded protein response: from stress pathway to homeostatic regulation. *Science* 2011;334:1081–1086.
23. Triolo D, Dina G, Taveggia C, et al. Vimentin regulates peripheral nerve myelination. *Development* 2012;139:1359–1367.
24. Miura H, Oda K, Endo C, et al. Progressive degeneration of motor nerve terminals in GAD mutant mouse with hereditary sensory axonopathy. *Neuropathol Appl Neurobiol* 1993;19:41–51.
25. Maraganore DM, Lesnick TG, Elbaz A, et al. UCHL1 is a Parkinson's disease susceptibility gene. *Ann Neurol* 2004;55:512–521.
26. Fink JK. Hereditary spastic paraplegia: clinico-pathologic features and emerging molecular mechanisms. *Acta Neuropathol* 2013;126:307–328.
27. Rainier S, Bui M, Mark E, et al. Neuropathy target esterase gene mutations cause motor neuron disease. *Am J Hum Genet* 2008;82:780–785.
28. Rossor AM, Kalmar B, Greensmith L, Reilly MM. The distal hereditary motor neuropathies. *J Neurol Neurosurg Psychiatry* 2012;83:6–14.
29. Sakurai M, Sekiguchi M, Zushida K, et al. Reduction in memory in passive avoidance learning, exploratory behaviour and synaptic plasticity in mice with a spontaneous deletion in the ubiquitin C-terminal hydrolase L1 gene. *Eur J Neurosci* 2008;27:691–701.
30. Gong B, Cao Z, Zheng P, et al. Ubiquitin hydrolase Uch-L1 rescues beta-amyloid-induced decreases in synaptic function and contextual memory. *Cell* 2006;126:775–788.
31. Wang L, Popko B, Tixier E, Roos RP. Guanabenz, which enhances the unfolded protein response, ameliorates mutant SOD1-induced amyotrophic lateral sclerosis. *Neurobiol Dis* 2014;71:317–324.
32. Lemus L, Goder V. Regulation of Endoplasmic Reticulum-Associated Protein Degradation (ERAD) by Ubiquitin. *Cells* 2014;3:824–847.
33. Benyair R, Ron E, Lederkremer GZ. Protein quality control, retention, and degradation at the endoplasmic reticulum. *Int Rev Cell Mol Biol* 2011;292:197–280.
34. Dupuis L, Loeffler JP. Neuromuscular junction destruction during amyotrophic lateral sclerosis: insights from transgenic models. *Curr Opin Pharmacol* 2009;9:341–346.
35. Valdez G, Tapia JC, Lichtman JW, et al. Shared resistance to aging and ALS in neuromuscular junctions of specific muscles. *PLoS ONE* 2012;7:e34640.
36. Morfini GA, You YM, Pollema SL, et al. Pathogenic huntingtin inhibits fast axonal transport by activating JNK3 and phosphorylating kinesin. *Nat Neurosci* 2009;12:864–871.

Supporting Information

Additional Supporting Information may be found in the online version of this article:

Figure S1. UCHL1 is expressed in the motor axons at the ventral root (A,B) and femoral nerve (C,D) level, but not the myelin sheets (S-100, green) wrapping around them.

Figure S2. There is no difference in the synaptic input on to calretinin+ interneurons in the spinal cord.

Figure S3. SMN of UCHL1^{-/-} mice do not display increased ER stress. PERK (A) and PDI (B) expression levels are comparable between WT and UCHL1^{-/-} SMN at P40 and P100.

Figure S4. There is progressive muscle atrophy in the absence of UCHL1 function.

Figure S5. pJNK levels are increased in spinal cord of UCHL1^{-/-} mice.